Journal of Alloys and Compounds 502 (2010) 445–450

Contents lists available at ScienceDirect

Journal of Alloys and Compounds

journal homepage: www.elsevier.com/locate/jallcom

The alloying effects on the structural and optical properties of nanocrystalline copper zinc oxide thin films fabricated by spin coating and annealing method

İbrahim Y. Erdoğan*

Bingöl University, Faculty of Sciences and Arts, Department of Chemistry, 12000 Bingöl, Turkey

ARTICLE INFO

Article history:
Received 18 March 2010
Received in revised form 9 April 2010
Accepted 25 April 2010
Available online 5 May 2010

Keywords:
Copper zinc oxide
Spin coating
Thin films
Nanostructures
Doping
Structural/optical properties

ABSTRACT

The present paper reports on a systematic study of the influence of Zn alloying on the structural and optical characteristics of CuZnO thin films. Nanocrystalline CuZnO thin films were prepared on p-type Si (1 0 0) substrates by spin coating from a CuO solution mixed with Zn of 0–8.0 at.%. All the prepared samples were annealed in oxygen gas atmosphere at 673 K for 2 h. A detailed characterization of the films doped with zinc was performed by X-ray diffraction (XRD), Fourier transform infrared (FT-IR) spectroscopy, ultraviolet–visible (UV–vis) spectroscopy, photoluminescence (PL) spectroscopy, atomic absorption spectroscopy (AAS), and energy dispersive X-ray spectroscopy (EDS). The structural analyses suggest that Zn successfully occupied the Cu sites and did not change the monoclinic structure of CuO. After 4.0 at.% Zn was doped, the crystalline quality and (0 0 2) preferential orientation of the thin film improved. However, when the Zn doping concentration was above 4.0 at.%, the crystalline quality and preferential orientation of the thin film weakened in turn. The XRD and FT-IR results showed single phase CuZnO for the lower (at.% $\leq$ 6.0) Zn concentration, while a secondary phase of ZnO evolved for 8.0 at.%. The optical band gap, determined from the absorbance spectra, showed a blue shift with increasing Zn content. The works showed that the structural and optical properties of CuO films doped with Zn can be improved and the 4.0 at.% Zn-doped CuO thin films have the best crystallization quality and the strongest emission ability.

1. Introduction

Due to an excess of oxygen, cupric oxide (CuO, copper (II) oxide) is a p-type semiconductor and exhibits a number of promising properties. However, CuO is one of the most important I–IV compound semiconductors with many applications, such as magnetic storage media [1], diode applications [2], field transistors [3], solar cells [4], photovoltaic applications [5], secondary batteries [6], superconductors [7], gas sensors [8], and so on.

The field of nanocrystalline semiconductor thin films has recently grown worldwide into a major research area [9]. These films are comprised of interconnected nanocrystallites that display unique chemical, physical, optical and structural properties as a result of energy quantization in three dimensions as known for individual semiconductor nanoparticles and pronounced surface effects. A variety of technological applications such as sensors, solar cells, thermoelectric and electrochromic devices can be developed on the basis of nanocrystalline semiconductor thin films [10–12]. Nanocrystalline thin films can be prepared by various methods. Methods such as spin coating [2], chemical bath deposition [13], electrodeposition [14] and pulsed laser deposition [15] have been used to prepare tenorite monoclinic CuO thin films.

In order to obtain better crystallization quality and better optical and electrical properties, researchers have performed doping in metal oxides. Zinc is an important transition metal element and Zn^{2+} has close ionic radius parameter to that of Cu^{2+}, which means that Zn can easily penetrate into CuO crystal lattice or substitute Cu position in the crystal. Zn-doped CuO crystals have previously been prepared by the floating-zone technique [16]. To the author's knowledge, no information is available in the literature on the preparation and characterization of Zn-doped CuO thin films.

In this study, the CuZnO thin films were fabricated by the spin coating and annealing method, which can produce economically feasible large area films with good crystalline and optic properties. These films were characterized using X-ray diffraction (XRD), Fourier transform infrared (FT-IR) spectroscopy, ultraviolet–visible (UV–vis) spectroscopy, photoluminescence (PL) spectroscopy, atomic absorption spectroscopy (AAS), and energy dispersive X-ray spectroscopy (EDS). The effects of Zn doping on the nanostructure and optical properties and their interplays in the CuO thin films are discussed in detail.

* Tel.: +90 426 2132550×1185.
E-mail address: ibrahimyerdogan@gmail.com.

0925-8388/$ – see front matter © 2010 Elsevier B.V. All rights reserved.
doi:10.1016/j.jallcom.2010.04.193

2. Experimental details

2.1. Chemicals and materials

Stock solutions of 100 mM $Cu(NO_3)_2$ (Aldrich 99.999% purity), 100 mM $Zn(NO_3)_2$ (Aldrich 99.999% purity) and 50 mM NaOH (Aldrich 99.999% purity) were used to fabricate thin films of copper zinc oxide. The stock solutions were prepared by dissolving $Zn(NO_3)_2$, $Cu(NO_3)_2$ and NaOH in deionized water (resistivity > 18 MΩ cm). The p-type Si (1 0 0) wafers were chemically cleaned using the RCA cleaning procedure before performing deposition. The first step of RCA cleaning was performed with a 1:1:6 solution of NH_3:H_2O_2:H_2O at 350 K for 10 min. The second step was performed with a 1:1:6 solution of HCl:H_2O_2:H_2O at 330 K for 10 min. The final step involved a short immersion in a 1:50 solution of HF:H_2O at 298 K. The p-type Si substrate is both cheap and easy obtainable substrate. P-type Si substrate is also very useful for determination of electronic transport properties of thin films.

2.2. Characterization

The X-ray diffraction (XRD) experiments for the CuZnO thin films on Si (1 0 0) were carried out in a Rigaku advance powder X-ray diffractometer using Cu Kα radiation (λ = 1.5405 Å), operating at 30 kV and 30 mA over a 2θ range of 30–70°. The XRD phases present in the deposits were identified with the help of the JCPDS-ICDD. The Fourier transform infrared (FT-IR) transmission spectra of the Zn-doped CuO thin films prepared on Si substrates were measured by using a Perkin Elmer Spectrum One FT-IR spectrometer in the spectral range of 400–800 cm^{-1} at room temperature. Absorbance spectra of deposited CuZnO films were measured by using a Perkin Elmer Lambda 35 model UV–vis spectrophotometer in the spectral range of 300–700 nm at room temperature. The photoluminescence (PL) spectra were measured at room temperature by using a Shimadzu RF-5301 PC Spectrofluorophotometer. The chemical compositions and stoichiometry of the films were determined by an energy dispersive X-ray spectrometer (EDS) with a JEOL-JSM-6060LV system and a Pelkin Elmer Aanalyst 800 atomic absorption spectrometer (AAS).

3. Results and discussion

3.1. Reaction mechanism and film formation

The dispersions containing copper zinc oxide solutions were spin coated and annealed on the Si (1 0 0) substrates. These dispersions were prepared as follows by a simple chemical method. 50 mM NaOH solutions were added dropwise in 100.0 mM $Cu(NO_3)_2$ + 0.0 mM $Zn(NO_3)_2$, 98.0 mM $Cu(NO_3)_2$ + 2.0 mM $Zn(NO_3)_2$, 96.0 mM $Cu(NO_3)_2$ + 4.0 mM $Zn(NO_3)_2$, 94.0 mM $Cu(NO_3)_2$ + 6.0 mM $Zn(NO_3)_2$ and 92.0 mM $Cu(NO_3)_2$ + 8.0 mM $Zn(NO_3)_2$ solutions under magnetic stirring condition (Table 1). The metal salt $Cu(NO_3)_2$ + $Zn(NO_3)_2$ and NaOH solutions were mixed in a ratio of 1:1 at 298 K. Addition of NaOH solution to $Cu(NO_3)_2$ + $Zn(NO_3)_2$ mixture produces precipitates of $Cu_{1-x}Zn_x(OH)_2$ as indicated in Eq. (1). These solutions containing $Cu_{1-x}Zn_x(OH)_2$ precipitates were heated at 360 K for 2 h. Heating $Cu_{1-x}Zn_x(OH)_2$ precipitates helps better crystallization of materials and the formation of $Cu_{1-x}Zn_xO$ particles, as shown in Eq. (2):

$$(1-x)Cu(NO_3)_2 + (x)Zn(NO_3)_2 + 2NaOH \rightarrow Cu_{1-x}Zn_x(OH)_2 + 2NaNO_3 \quad (1)$$

$$Cu_{1-x}Zn_x(OH)_2 \rightarrow Cu_{1-x}Zn_xO + H_2O \quad (2)$$

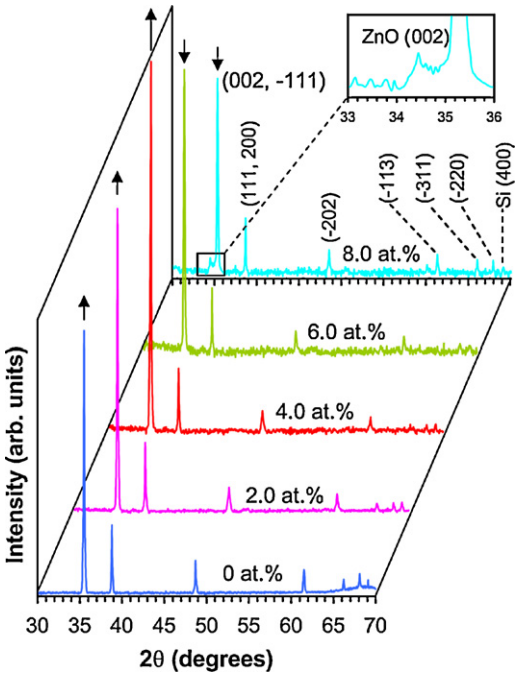

Fig. 1. XRD patterns of CuZnO thin films for various Zn doping concentrations.

The as-obtained precipitates were washed with deionized water and dried. The dried copper zinc oxide particles were dispersed in non-polar organic solvents like hexane. The dispersions were added onto the Si substrates using a pipette. The silicon substrates were spin-coated at 1000 rpm and then accelerated to the final rotation speed. The final rotation speed was adjusted to 3000 rpm for 25 s. After coating, the samples were annealed in oxygen atmosphere at 673 K for 3 h. The optimum annealing temperature for preparation of the alloy films that have best crystallization quality was determined as 673 K.

The thickness of CuZnO films on Si substrate was determined by a gravimetric weight difference method in conjunction with Eq. (3):

$$t = \frac{M}{\rho A} \quad (3)$$

where M is the mass of the film on the substrate (g), A is the surface area of the film (cm^2) and ρ is the bulk density of the prepared material (CuO = 6.310 g/cm^3, $Cu_{0.98}Zn_{0.02}O$ = 6.296 g/cm^3, $Cu_{0.96}Zn_{0.04}O$ = 6.282 g/cm^3, $Cu_{0.94}Zn_{0.06}O$ = 6.268 g/cm^3, $Cu_{0.92}Zn_{0.08}O$ = 6.254 g/cm^3, ZnO = 5.606 g/cm^3). Here, the thickness of all CuZnO thin films was approximately calculated as 120 nm with a standard deviation of 5 nm.

3.2. Structural studies

Fig. 1 shows the XRD patterns of undoped (pure) and doped CuO thin films with different concentrations of zinc. All the peaks

Table 1
The mixed solutions (solutions were mixed in a ratio of 1:1) and prepared compounds.

Mixed solutions		Prepared compounds	
Metal salt solution	NaOH solution	Before heating	After heating
100.0 mM $Cu(NO_3)_2$ + 0.0 mM $Zn(NO_3)_2$	50 mM NaOH	$Cu(OH)_2$	CuO
98.0 mM $Cu(NO_3)_2$ + 2.0 mM $Zn(NO_3)_2$	50 mM NaOH	$Cu_{0.98}Zn_{0.02}(OH)_2$	$Cu_{0.98}Zn_{0.02}O$
96.0 mM $Cu(NO_3)_2$ + 4.0 mM $Zn(NO_3)_2$	50 mM NaOH	$Cu_{0.96}Zn_{0.04}(OH)_2$	$Cu_{0.96}Zn_{0.04}O$
94.0 mM $Cu(NO_3)_2$ + 6.0 mM $Zn(NO_3)_2$	50 mM NaOH	$Cu_{0.94}Zn_{0.06}(OH)_2$	$Cu_{0.94}Zn_{0.06}O$
92.0 mM $Cu(NO_3)_2$ + (8.0 mM $Zn(NO_3)_2$	50 mM NaOH	$Cu_{0.92}Zn_{0.08}(OH)_2$	$Cu_{0.92}Zn_{0.08}O$

in the patterns of undoped CuO correspond to the tenorite monoclinic CuO phase and are in close agreement with the JCPDS-ICDD standard (No. 05-0661, 13-0420, 45-0937, 48-1548) cards of the monoclinic CuO (space group: $C2/c$) structure with lattice parameters $a = 4.68$ Å, $b = 3.42$ Å, $c = 5.13$ Å and $\beta = 99.5°$. As seen in the patterns, both pure and Zn-doped CuO thin films show a strong diffraction peak corresponding to the (0 0 2) plane. The weak peak at 69.1° corresponds to (4 0 0) reflection of Si (JCPDS-ICDD No. 27-1402), which belongs to the substrate in this work. Other weak diffraction peaks correspond to (1 1 1 and 2 0 0), (−2 0 2), (−1 1 3), (−3 1 1) and (−2 2 0) reflections of CuO. Zn^{2+} (74 pm) has close ionic radius to that of Cu^{2+} (73 pm), which means that Zn can easily penetrate into CuO crystal lattice or substitute Cu position in the crystal. Thus, single-phase CuZnO was observed for the lower (at.% ≤ 6.0) Zn concentration. However, when Zn doping concentration was 8.0 at.%, a weak peak appeared at around 34.4°, corresponding to the (0 0 2) peak of ZnO (JCPDS-ICDD No. 36-1451). It was revealed that a secondary phase of ZnO evolved when the high concentration of Zn (at.% ≥ 8) was doped into CuO thin films (Fig. 1). Prabhakaran and Boothroyd [16] have recently reported that Zn-doped CuO crystals could be fabricated by the floating-zone method. They demonstrated that a single phase was formed for 5 at.% Zn concentration, while a secondary phase of ZnO was observed for 10 at.%. As a result of the lattice mismatch, the oxygen ions were drawn to the zinc ions to form the ZnO, which is highly in harmony with the results obtained from FT-IR measurements. When the Zn doping concentration was 4.0 at.%, the diffraction intensity of (0 0 2) peak was the strongest. The intensity ratios for (0 0 2) and (1 1 1) reflections ($I_{(002)}/I_{(111)}$) of undoped and 4.0 at.% Zn-doped thin films were 3.72 and 5.37, respectively (Fig. 2). For a powder sample, the $I_{(002)}/I_{(111)}$ is 1.098 (JCPDS-ICDD No. 45-0937). From the above results, it is apparent that 4.0 at.% Zn doping greatly improved the crystallization quality of the thin films, but the crystallization quality dropped when Zn doping concentration was above 4.0 at.%. In addition, the location of the (0 0 2) peaks shifted to lower 2θ angles, from 35.5° to 35.3° as Zn doping content increased from 0 to 8.0 at.% (Fig. 3). Fig. 3 also shows the change in the lattice constant (d value) with increasing Zn doping. The shift in the peak implies systematical incorporation of the Zn^{2+} ions for the Cu^{2+} ions in the lattice without changing its monoclinic structure. After 8.0 at.% Zn was doped, a lattice mismatch emerged between CuO and ZnO. The full width at half maximum (FWHM) of the diffraction peaks from CuZnO thin films are broader than those of pure CuO films, which illustrates that Zn doping can appreciably influence CuO crystallinity (Fig. 4). The FWHM, the width at half maximum peak intensity, is inversely proportional to the crystal size and can

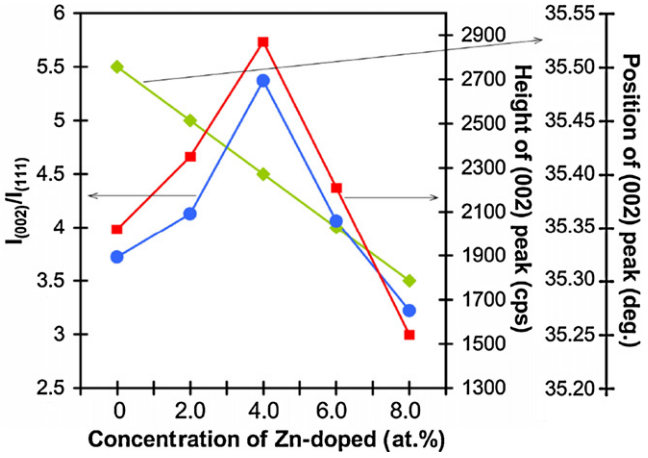

Fig. 2. Changes of the parameter of XRD peak of the films with different Zn concentrations.

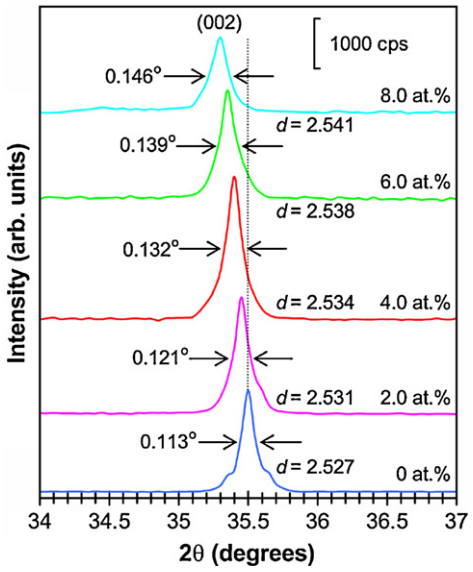

Fig. 3. Plot of shifting of (0 0 2) peak positions for CuZnO films with different compositions.

be related to the quality of crystallinity in thin films [17]. The effect of Zn dopant concentration on the crystallinity and crystal size of the films was determined by Scherrer's formula [18]:

$$D = \frac{0.9\lambda}{(\mathrm{FWHM})\cos\theta} \quad (4)$$

where D is the crystal size of the prepared thin films, λ is the X-ray wavelength (0.154 nm) and θ is the Bragg diffraction angle. The calculated average crystallite sizes of 0, 2.0, 4.0, 6.0 and 8.0% Zn-doped CuO thin films were 74, 69, 63, 60 and 57 nm, respectively (Fig. 4). The results imply that the grain size of nanocrystalline thin films decrease with increasing Zn content.

Fig. 5 presents the FT-IR spectra of undoped and four CuO thin films with different Zn compositions. The infrared spectra show the specific vibration mode determined by the selection rule [19]. The FT-IR spectrum of undoped CuO consists of peaks at 431, 480, 529, 606 and 615 cm^{-1}. The IR peaks at 431, 480, 529 and 606 cm^{-1} correspond to characteristic stretching vibrations of Cu–O bond in CuO [20,21]. The IR peak at 615 cm^{-1} belongs to Si [2,22]. However, when Zn doping concentration was 8.0 at.%, an IR peak appeared at around 460 cm^{-1}. The intensity of this IR peak increased when the high concentration of Zn (at.% > 8) was doped into CuZnO thin films. Thus, it was concluded that the IR peak at 460 cm^{-1} corre-

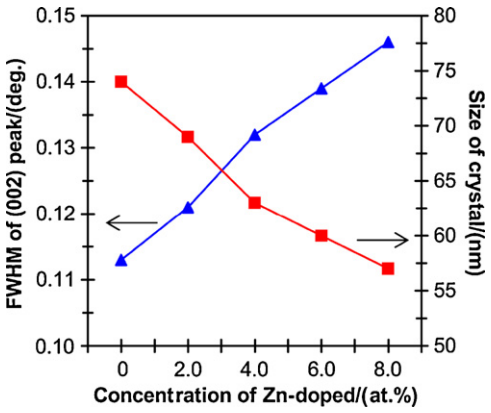

Fig. 4. Changes of the FWHM and crystal size in the CuZnO films with different Zn contents.

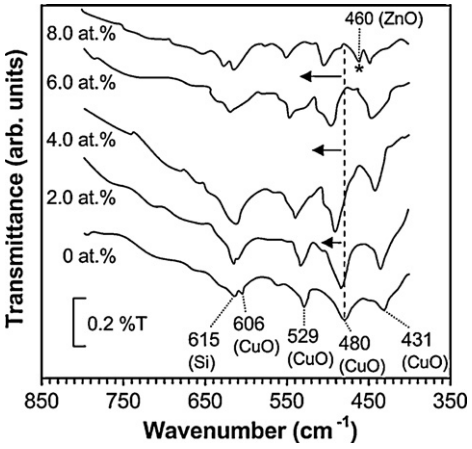

Fig. 5. FT-IR spectra of the CuZnO thin films with various Zn doping contents.

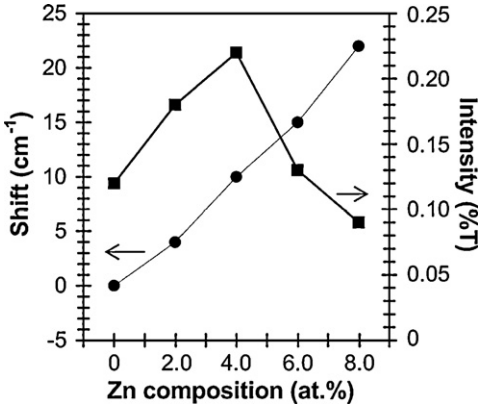

Fig. 6. Changes of the peak frequency and intensity of films as a function of Zn composition.

sponds to characteristic stretching vibrations of Zn–O bond [23]. As seen in Fig. 5, the IR peaks shifted to higher energy or frequency (about 25 cm^{-1}) as the Zn composition increased. In the simple form of the two-atom interaction model, the peak wavenumber is a function of the bond strength and reduced mass [24]. In the present case, it is concluded that Zn substitution strengthens the chemical bond in the lattice, because the mass of substituting element Zn (65.384 g/mol) is larger than the reduced mass of CuO (12.781 g/mol). The reduced mass μ of CuO was calculated by Eq. (5):

$$\mu_{CuO} = \frac{m_{Cu} m_O}{m_{Cu} + m_O} \quad (5)$$

where m_{Cu} and m_O are the masses of Cu and O. Moreover, the blue shift of the IR peaks in CuZnO alloys may result from the fact that Cu–O bonds undergo a compressive strain because of the lattice mismatch between CuO and ZnO, which increases the effective force constant referred to as compositional disorder of the alloy [25]. Fig. 6 shows the change in the peak frequency and intensity of alloy thin films as a function of Zn composition. When the Zn doping concentration was 4.0 at.%, the intensity of the IR peaks was the strongest. It is apparent that 4.0 at.% Zn doping greatly improved crystal quality, but crystal quality was reduced when Zn doping concentration was above 4.0 at.%. The FT-IR results are highly consistent with the XRD results. Both XRD and FT-IR studies did not showed any oxidation layer such as silicon oxide.

The chemical compositions and stoichiometry of the alloy films were determined by EDS (for Cu, Zn and O) and AAS (for Cu and Zn) techniques. All the EDS and AAS data are given in Table 2. As shown in Table 2, atomic percentage of the Cu:Zn in thin films is in close agreement with the molar ratio of the elemental precursors taken in the solution during coating. It was found that the quantitative atomic ratio of (Cu + Zn) and O are approximately 50% versus 50% for $Cu_{1-x}Zn_xO$ thin films, a ratio which is close to 1:1 stoichiometries.

3.3. Optical studies

Fig. 7 shows the optical absorption spectra of CuZnO thin films with various zinc doping concentrations in the range of 300–700 nm. The band edge for all these films is in the range of 470–446 nm. The absorption wavelength of the alloy thin films decreased with Zn doping. In other words, the absorption edge blue shifted toward higher energy sides for the CuO thin films formed at higher ZnO doping levels. This indicates that the band gap of CuZnO material increases with increasing Zn doping concentration. Since the band gap of ZnO (3.37 eV) [26] is higher than that of CuO, so the

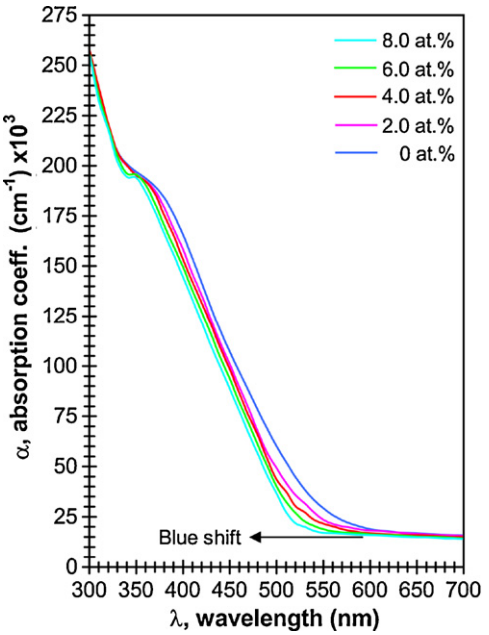

Fig. 7. Absorption spectra of CuZnO thin films with the various zinc doping concentrations.

Table 2
The chemical compositions and stoichiometry.

Formula	The molar percentage in the solution (mM)		The atomic percentage in films by EDS (Cu/Zn/O)			The atomic percentage in films by AAS (Cu/Zn)	
	$Cu(NO_3)_2$	$Zn(NO_3)_2$	Cu	Zn	O	Cu	Zn
CuO	100.0	0.0	48.8	0.0	51.2	100.0	0.0
$Cu_{0.98}Zn_{0.02}O$	98.0	2.0	47.1	1.2	51.7	97.7	2.3
$Cu_{0.96}Zn_{0.04}O$	96.0	4.0	45.9	2.0	52.1	95.8	4.2
$Cu_{0.94}Zn_{0.06}O$	94.0	6.0	44.5	3.1	52.4	93.6	6.4
$Cu_{0.92}Zn_{0.08}O$	92.0	8.0	44.2	3.9	51.9	91.7	8.3

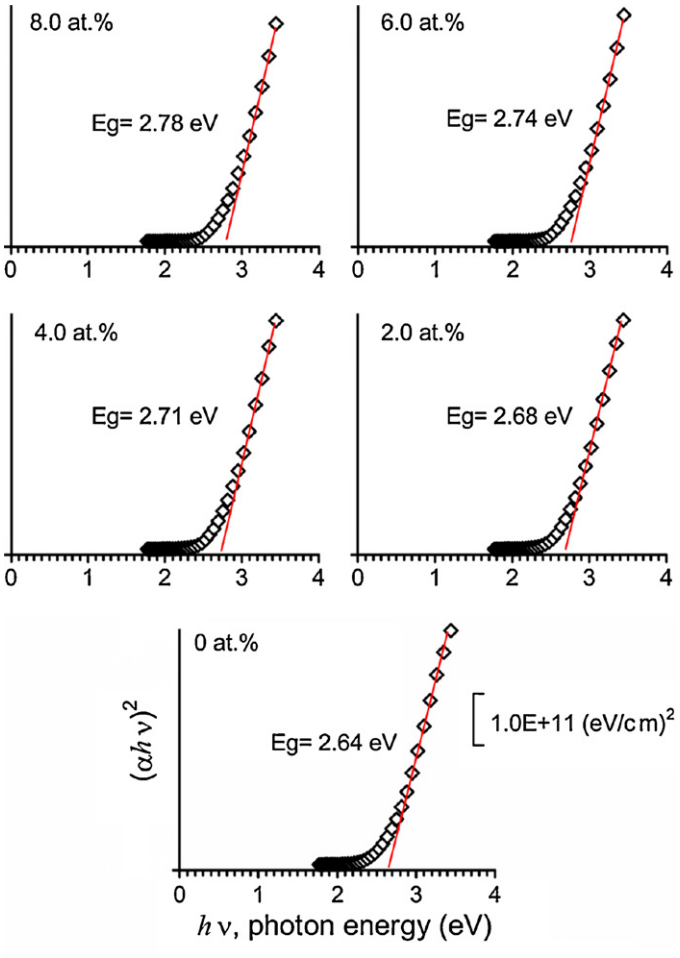

Fig. 8. Plot of $(\alpha h\upsilon)^2$ vs. $(h\upsilon)$ for CuZnO films with different compositions.

band gap of CuZnO should be greater than the band gap of CuO. The optical results were analyzed using the following relationship (Eq. (6)):

$$\alpha h\upsilon = B(h\upsilon - E_g)^m \quad (6)$$

where B is a constant, E_g is the optical band gap, α is the absorption coefficient of the film, which was calculated from the optical absorbance (A) and thickness (d) of the thin film according to Eq. (7) [2,27]:

$$A = 0.434\alpha d \quad (7)$$

The exponent m depends on the nature of the transition, $m = 1/2$, 2, 3/2, or 3 for allowed direct, allowed non-direct, forbidden direct or forbidden non-direct transitions, respectively. The optical absorption or absorption coefficient ($\alpha \geq 10^4\ cm^{-1}$) is related to direct band transitions [28–30].

Fig. 8 shows the plot of $(\alpha h\upsilon)^2$ vs. $(h\upsilon)$ according to Eq. (6). Satisfactory fit is obtained for $(\alpha h\upsilon)^2$ vs. $(h\upsilon)$ indicating the presence of a direct band gap. The optical band gaps of undoped and 8.0% Zn-doped CuO films were respectively determined as 2.64 eV and 2.78 eV by extrapolating the linear portion of these plots at $(\alpha h\upsilon)^2 = 0$, which indicates that the direct allowed transition dominates in the undoped and Zn-doped CuO films. The optical band gap value obtained for pure CuO is consistent with the value of 2.60 eV reported by Liu et al. [31] and 2.75 eV reported by Zhang et al. [32]. The optical band gap increased from 2.64 to 2.78 eV as Zn concentration increased in the CuZnO films. Fig. 9 shows the band gap dependency of CuZnO thin films as a function of the composition.

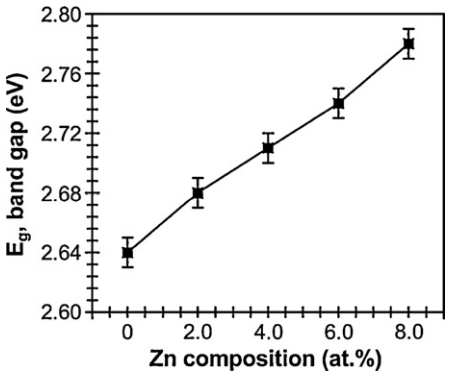

Fig. 9. Band gap dependency of CuZnO thin films as a function of the composition.

These results clearly demonstrate that the band gap of nanocrystalline thin films is directly related to the film composition. Recent advances in semiconductor nanocrystals or nanocrystalline thin films such as CuZnO have shown that their band gaps can be tuned by changing their constituent stoichiometries. According to Vegard's Law [33], the optical band gap of alloys varies linearly with material composition according to Eq. (8):

$$E_{g(\text{alloy},A_xB_{1-x})} = xE_{g(A)} + (1-x)E_{g(B)} \quad (8)$$

where x is the mole fraction, E_{alloy}, E_A and E_B are the optical band gap energy values of the alloy A_xB_{1-x}, pure A and pure B materials, respectively.

Fig. 10 presents the room temperature PL spectra of CuZnO films prepared on Si substrates. The emission properties of undoped and Zn-doped CuO films were studied by using PL spectra excited with 335 nm. The PL spectra of the alloy films show a broad emission band centered at about 465 nm (2.67 eV). These broad blue range emission peaks are attributed to the near-band edge emission (NBE). Similarly, Kim and co-workers [34] demonstrated that the emission of the PL spectrum for CuO nanoparticles is observed in the blue region. As the Zn concentration increased, the position of the PL peak at the 465 nm remained unchanged, and the emission intensity of this peak changed. The intensity of blue NBE emission depends strongly on Zn concentration. When doped with 2.0 and 4.0 at.% Zn, the thin films exhibit more intense blue emission than undoped CuO film, and the intensity of blue NBE emission decreases with further increase (at.% ≥ 6.0) of the Zn dopant. The blue NBE emission spectra from exciton-related recombination [35,36]. The quenching of emission may imply that some nonradiative recombi-

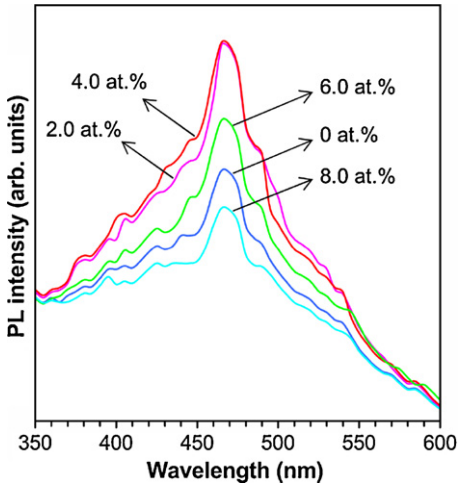

Fig. 10. PL spectra for CuZnO films doped with different Zn concentrations.

nation process occurred in the thin films. Similar phenomena were observed in Cu-doped ZnO films [37]. When CuO thin film are doped with 2.0 and 4.0 at.% Zn, they could be considered to exist as interstitials that share the oxygen with Cu atoms and hence decrease the defects of O vacancies or O interstitials, which leads to the enhancement of NBE emission. With further increase of Zn doping concentration, the intensity of NBE emission declines. As a result, the structural and optical data showed that the 4.0 at.% Zn-doped CuO thin films had the best crystallization quality and the strongest emission ability.

4. Conclusions

Nanocrystalline CuZnO thin films were prepared on p-type Si (1 0 0) substrates by spin coating and annealing method. The structural analyses of prepared films suggest that Zn successfully occupied the Cu sites and did not change the monoclinic structure of CuO. When 4.0 at.% Zn was doped, the crystalline quality and (0 0 2) preferential orientation of the thin film improved. However, when the doping concentration was above 4.0 at.%, the crystalline quality and the preferential orientation of the film decreased. The structural results showed single-phase CuZnO for the lower (at.% $\leq$ 6.0) Zn concentration, while a secondary phase of ZnO evolved for 8.0 at.%. The band gap of alloy films showed a blue shift with increasing Zn content. The results showed that the 4.0 at.% Zn-doped CuO thin films had the best crystallization quality and the strongest emission ability. As a result, it can be argued that the structural and optical properties of alloy thin films can be improved by Zn doping.

Acknowledgements

The author gratefully acknowledges financial supports from Bingol University and the author wants to thank Dr. Kadem Meral for the PL analysis.

References

[1] T.I. Arbuzova, B.A. Gizhevskii, S.V. Naumov, A.V. Korolev, V.L. Arbuzov, K.V. Shalnov, A.P. Druzhkov, J. Magn. Magn. Mater. 258 (2003) 342.
[2] I.Y. Erdogan, O. Gullu, J. Alloys Compd. 492 (2010) 378.
[3] E.M. Alkoy, P.J. Kelly, Vacuum 79 (2005) 221.
[4] T. Maruyama, Sol. Energy Mater. Sol. Cells 56 (1998) 85.
[5] E. Vigil, F.A. Fernandez-Lima, J.A. Ayllon, E. Pedrero, I. Zumeta, B. Gonzalez, L. Curbelo, H.D. Fonseca-Filho, M.E.H. Maia da Costa, C. Domingo, M. Behar, F.C. Zawislak, Micropor. Mesopor. Mater. 109 (2008) 560.
[6] X.P. Gao, J.L. Bao, G.L. Pan, H.Y. Zhu, P.X. Huang, F. Wu, D.Y. Song, J. Phys. Chem. B 108 (2004) 5547.
[7] X.G. Zheng, C.N. Xu, Y. Tomokiyo, E. Tanaka, H. Yamada, Y. Soejima, Phys. Rev. Lett. 85 (2000) 5170.
[8] Y. Li, J. Liang, Z. Tao, J. Chen, Mater. Res. Bull. 43 (2008) 2380.
[9] C.D. Lokhande, A.M. More, J.L. Gunjakar, J. Alloys Compd. 486 (2009) 570.
[10] B. O'Reagan, M. Gratzel, Nature 353 (1991) 737.
[11] R. Venkatasubramanian, E. Siivola, T. Colpitts, B. O'Quinn, Nature 413 (2001) 597.
[12] A. Hagfeldt, N. Vlachopoulos, M. Gratzel, J. Electrochem. Soc. 141 (1994) 181.
[13] D.P. Dubal, D.S. Dhawale, R.R. Salunkhe, V.S. Jamdade, C.D. Lokhande, J. Alloys Compd. 492 (2010) 26.
[14] E.W. Bohannan, I.M. Nicic, H.M. Kothari, J.A. Switzer, Electrochim. Acta 53 (2007) 155.
[15] A. Chen, G. Yang, H. Long, F. Li, Y. Li, P. Lu, Thin Solid Films 517 (2009) 4277.
[16] D. Prabhakaran, A.T. Boothroyd, J. Cryst. Growth 250 (2003) 77.
[17] M. Maniv, A. Zangvil, J. Appl. Phys. 49 (1978) 2787.
[18] B.D. Cullity, Elements of X-ray Diffractions, Addison-Wesley, Reading, MA, 1978, p. 102.
[19] K. Nakamoto, Infrared and Raman Spectra of Inorganic and Coordination Compounds, John Wiley-Sons, New York, 1986.
[20] M.A. Dar, Y.S. Kim, W.B. Kim, J.M. Sohn, H.S. Shin, Appl. Surf. Sci. 254 (2008) 7477.
[21] B. Balamurugan, B.R. Mehta, Thin Solid Films 396 (2001) 90.
[22] K.P. Muthe, J.C. Vyas, S.N. Narang, D.K. Aswal, S.K. Gupta, D. Bhattacharya, R. Pinto, G.P. Kothiyal, S.C. Sabharwal, Thin Solid Films 324 (1998) 37.
[23] G. Guoa, C. Shia, D. Taoa, W. Qianb, D. Han, J. Alloys Compd. 472 (2009) 343.
[24] M. Nakayama, M. Kaneko, Y. Uchimoto, M. Wakihara, K. Kawamura, J. Phys. Chem. B 108 (2004) 3754.
[25] C. Ramkumar, K.P. Jain, S.C. Abbi, Phys. Rev. B 54 (1996) 7921.
[26] B. Kulyk, B. Sahraoui, V. Figa, B. Turko, V. Rudyk, V. Kapustianyk, J. Alloys Compd. 481 (2009) 819.
[27] N.F. Mott, R.W. Gurney, Electronic Processes in Ionic Crystals, Oxford U. Press, London, 1940.
[28] A.K. Abass, A. Krier, R.A. Collins, Phys. Stat. Sol. (a) 142 (1994) 435.
[29] K.R. Rajesh, C.S. Menon, Eur. Phys. J. B 47 (2005) 171.
[30] O. Gullu, A. Turut, Sol. Energy Mater. Sol. Cells 92 (2008) 1205.
[31] Q. Liu, H. Liu, Y. Liang, Z. Xu, G. Yin, Mater. Res. Bull. 41 (2006) 697.
[32] X. Zhang, D. Zhang, X. Ni, H. Zheng, Solid-State Electron. 52 (2008) 245.
[33] A.R. Denton, N.W. Ashcroft, Phys. Rev. A 43 (1991) 3161.
[34] D.I. Son, C.H. You, T.W. Kim, Appl. Surf. Sci. 255 (2009) 8794.
[35] J.J. Hopfield, D.G. Thomas, Phys. Rev. 122 (1961) 35.
[36] D.C. Reynolds, D.C. Look, B. Jobai, C.W. Litton, T.C. Collins, W. Harsch, G. Cantwell, Phys. Rev. B 57 (1998) 12151.
[37] X.B. Wang, C. Song, K.W. Geng, F. Zeng, F. Pan, Appl. Surf. Sci. 253 (2007) 6905.